[Reply on RC1]

We are very grateful to the referee #1 for the useful comments. They help to improve the paper quality. Below, we will reply to the specific comments.

Specific major comments

[1] One of the most important aspect of the paper is that the DFS expansion coefficients ($T^{\mathrm{c}}_{n,m}$, $T^{\mathrm{s}}_{n,m}$) are calculated based on the least square method, as is shown section 2.3. I am afraid, however, that the derivation procedure does not seem to be the least square method which is required for determining the expansion coefficients. The residual function here is defined using the difference between the spectral representation of the function (T^{c}_{m}, T^{s}_{m}) two different sets of DFS. The fact that, for the spherical harmonics model (SHM), the spectral coefficients are determined in the least square sense on the spherical domain is explained as below:

$$E \equiv \int_0^{\pi} \left[T^{\mathrm{c}}_m(\theta) - \sum_{n=m}^{N} c_n P^{\mathrm{m}}_n(\theta) \right]^2 \sin\theta \, d\theta \tag{Q1}$$

$$\frac{\partial E}{\partial c_n} = 0 \ \ldots \ \text{least squares error} \tag{Q2}$$

$$2 \int_0^{\pi} P^{\mathrm{m}}_n(\theta) \left[T^{\mathrm{c}}_m(\theta) - \sum_{n=m}^{N} c_n P^{\mathrm{m}}_n(\theta) \right] \sin\theta \, d\theta = 0 \tag{Q3}$$

$$\therefore c_n = \int_0^{\pi} P^{\mathrm{m}}_n(\theta) T^{\mathrm{c}}_m(\theta) \sin\theta \, d\theta \tag{Q4}$$

$$\left[\because \int_0^{\pi} P^{\mathrm{m}}_n(\theta) P^{\mathrm{m}}_{n'}(\theta) \sin\theta \, d\theta = \delta_{nn'} \right] \tag{Q5}$$

That is, c_n is obtained with least squared error on the sphere.

The least square method for the SHM in the present study is different from above equations.

From Eq. (R18) below (fixed from Eq (37)), Eqs. (30) and (31), and from $\partial E^{\mathrm{SH}} / \partial T^{\mathrm{c,SH}}_{n,m} = 0$, we can derive Eq. (34). Equation (34) is similar to Eq. (Q4), but $\tilde{T}^{\mathrm{c},J}_m(\theta)$ is used instead of $T^{\mathrm{c}}_m(\theta)$. The referee probably considers the difference between $\tilde{T}^{\mathrm{c},J}_m(\theta)$ and $T^{\mathrm{c}}_m(\theta)$ as a problem. The use of Eq. (34) is one way to calculate the expansion coefficients of Legendre functions (e.g., Sneeuw and Bun, 1996), although the coefficients calculated from Eq. (34) are different from those calculated from Eq. (Q4) with Gaussian quadrature (or Clenshaw–Curtis quadrature), that is,

$$\int_0^{\pi} P^{\mathrm{m}}_n(\theta) T^{\mathrm{c}}_m(\theta) \sin\theta \, d\theta \neq \int_0^{\pi} P^{\mathrm{m}}_n(\theta) \tilde{T}^{\mathrm{c},J}_m(\theta) \sin\theta \, d\theta . \tag{R1}$$

On the other hand, when we use sine series (for odd m) as basis functions, $\tilde{T}^{\mathrm{c}}_{n,m}$ in Eq. (19) is calculated by the forward Fourier sin transform as

$$\tilde{T}^{\mathrm{c}}_{n,m} = \frac{2}{\pi}\int_0^{\pi} \sin n\theta \, T^{\mathrm{c}}_m(\theta) d\theta . \tag{R2}$$

From Eq. (19),

$$\frac{2}{\pi}\int_0^{\pi} \sin n\theta \, \tilde{T}^{\mathrm{c},J}_m(\theta) d\theta = \tilde{T}^{\mathrm{c}}_{n,m} \tag{R3}$$

is also derived. Therefore,

$$\frac{2}{\pi}\int_0^{\pi} \sin n\theta \, T^{\mathrm{c}}_m(\theta) d\theta = \frac{2}{\pi}\int_0^{\pi} \sin n\theta \, \tilde{T}^{\mathrm{c},J}_m(\theta) d\theta \left(= \tilde{T}^{\mathrm{c}}_{n,m}\right) \tag{R4}$$

is satisfied. Eq. (R4) is in contrast to Eq. (R1).

From Eqs. (R4) and (A2c),

$$\frac{2}{\pi}\int_0^{\pi} \sin^2\theta \sin n\theta \, T^{\mathrm{c}}_m(\theta) d\theta = \frac{2}{\pi}\int_0^{\pi} \sin^2\theta \sin n\theta \, \tilde{T}^{\mathrm{c},J}_m(\theta) d\theta \tag{R5}$$

is derived. From Eqs. (R4) and (R5), $\tilde{T}^{\mathrm{c},J}_m(\theta)$ in Eq. (R7) below for odd $m\ (\geq 3)$ can be changed to $T^{\mathrm{c}}_m(\theta)$. The same thing can be said for other m. Therefore, in Eq. (21), $\tilde{T}^{\mathrm{c},J}_m(\theta)$ can be changed to $T^{\mathrm{c}}_m(\theta)$. This is important and we will describe this in the paper (or in the supplement).

[2] It looks like that the equations (24a)-(24d) are just algebraic equations resulted from simply multiplying $\sin\theta$ or $\sin^2\theta$ or $\sin^4\theta$ to the same equation. For instance, in the case of odd $m\ (\geq 3)$, it follows:

$$\boldsymbol{T^{\mathrm{c}}_m(\theta) = \sum_n T^{\mathrm{c}}_{n,m} \sin^2\theta \sin n\theta}$$

$$\boldsymbol{= \sum_n \tilde{T}^{\mathrm{c}}_{n,m} \sin n\theta} \tag{Q6}$$

$$\boldsymbol{\sin^2\theta \, T^{\mathrm{c}}_m(\theta) = \sum_n T^{\mathrm{c}}_{n,m} \sin^4\theta \sin n\theta}$$

$$\boldsymbol{= \sum_n \tilde{T}^{\mathrm{c}}_{n,m} \sin^2\theta \sin n\theta} \tag{Q7}$$

$$\boldsymbol{\sum_n T^{\mathrm{c}}_{n,m} \sin^4\theta \sin n\theta = \sum_n h^{\mathrm{c}}_{n,m} \sin n\theta} \tag{Q8}$$

$$\boldsymbol{\Rightarrow \underbrace{\begin{bmatrix} 5-diagonal \\ matrix \end{bmatrix}\begin{bmatrix} T^{\mathrm{c}}_{1,m} \\ T^{\mathrm{c}}_{3,m} \\ T^{\mathrm{c}}_{5,m} \\ \vdots \end{bmatrix}}_{\text{lhs of } (24d)} = \begin{bmatrix} h^{\mathrm{c}}_{1,m} \\ h^{\mathrm{c}}_{3,m} \\ h^{\mathrm{c}}_{5,m} \\ \vdots \end{bmatrix}} \tag{Q9}$$

$$\boldsymbol{\sum_n \tilde{T}^{\mathrm{c}}_{n,m} \sin^2\theta \sin n\theta = \sum_n h^{\mathrm{c}}_{n,m} \sin n\theta} \tag{Q10}$$

$$\Rightarrow \underbrace{\begin{bmatrix} \mathbf{3-diagonal} \\ \mathbf{matrix} \end{bmatrix}\begin{bmatrix} \tilde{\boldsymbol{T}}^{\mathbf{c}}_{\mathbf{1},\boldsymbol{m}} \\ \tilde{\boldsymbol{T}}^{\mathbf{c}}_{\mathbf{3},\boldsymbol{m}} \\ \tilde{\boldsymbol{T}}^{\mathbf{c}}_{\mathbf{5},\boldsymbol{m}} \\ \vdots \end{bmatrix}}_{\textbf{rhs of } (\mathbf{24}\boldsymbol{d})} = \begin{bmatrix} \boldsymbol{h}^{\mathbf{c}}_{\mathbf{1},\boldsymbol{m}} \\ \boldsymbol{h}^{\mathbf{c}}_{\mathbf{3},\boldsymbol{m}} \\ \boldsymbol{h}^{\mathbf{c}}_{\mathbf{5},\boldsymbol{m}} \\ \vdots \end{bmatrix} \qquad (\mathbf{Q11})$$

It should be explained why above equations are the same as those the author derived.

For instance, in the case of odd m (≥ 3), the following equation are obtained from Eqs. (27a), (28), (29) and (21):

$$\frac{1}{2\pi^2}\int_0^{2\pi}\int_0^{\pi}(\sin^2\theta\sin n\theta)\cos m\lambda\left[\sum_{m=0}^{M}\left(T_m^{\mathrm{c},N}(\theta)-\tilde{T}_m^{\mathrm{c},J}(\theta)\right)\cos m\lambda\right]d\theta d\lambda = 0$$
$$(n = 1,\dots,N-2) \qquad \text{(R6)}$$

From Eq. (R6),

$$\frac{1}{2\pi}\int_0^{\pi}\sin^2\theta\sin n\theta\left(T_m^{\mathrm{c},N}(\theta)-\tilde{T}_m^{\mathrm{c},J}(\theta)\right)d\theta = 0 \qquad \text{(R7)}$$

is derived. From Eqs. (R7), (8a) and (19), we derive

$$\frac{1}{2\pi}\int_0^{\pi}\sin n\theta\left[\sum_{n=1}^{N-2}T_{n,m}^{\mathrm{c}}\sin^4\theta\sin n\theta-\sum_{n=1}^{J}\tilde{T}_{n,m}^{\mathrm{c}}\sin^2\theta\sin n\theta\right]d\theta = 0. \qquad \text{(R8)}$$

Here, we define $h_{n,m}^{\mathrm{c}}$ and $\tilde{h}_{n,m}^{\mathrm{c}}$ as

$$\sum_{n=1}^{N+2}h_{n,m}^{\mathrm{c}}\sin n\theta \equiv \sum_{n=1}^{N-2}T_{n,m}^{\mathrm{c}}\sin^4\theta\sin n\theta, \qquad \text{(R9)}$$

$$\sum_{n=1}^{J+2}\tilde{h}_{n,m}^{\mathrm{c}}\sin n\theta \equiv \sum_{n=1}^{J}\tilde{T}_{n,m}^{\mathrm{c}}\sin^2\theta\sin n\theta. \qquad \text{(R10)}$$

From Eqs. (R8), (R9) and (R10), we obtain

$$h_{n,m}^{\mathrm{c}} = \tilde{h}_{n,m}^{\mathrm{c}} \qquad (n = 1,..,N-2). \qquad \text{(R11)}$$

Thus, Eqs. (Q8), (Q9), (Q10) and (Q11) are derived. This is interesting. We will describe this in the paper or in the supplement.

[3] The largest wavenumber (truncation wavenumber) in (8b) should be determined considering the grid structure, grid[0] or grid[1] or grid[-1] to make completeness of spectral expansion issue clear (refer to Cheong et al. 2004).

Thank you for the advice. In the old DFS method using the Cheong's basis functions in Eq. (6) with Grid [0], N can be up to J^0-1 for $m=0$, and J^0 for $m\neq 0$ (Cheong et al. 2004). In the new DFS method using Eqs. (8), (19), (53) and (54) with Grid [0], N can be up to J^0-1 for each m because Eq. (66) is used for a scalar variable when m is even and vector components when m is

odd. In the new DFS method with Grid [1], N can be up to J^0-1 for each m because Eq. (69) is used for a scalar variable when m is odd and vector components when m is even. In the new DFS method with Grid [−1], N can be up to J^0-1 for $m \geq 2$ because Eq. (69) is used for a scalar variable when $m\ (\geq 3)$ is odd and vector components when $m\ (\geq 2)$ is even. With Grid [−1], N can be up to J^0-2 for $m = 0,1$ because Eqs. (73) and (75) are used for a scalar variable when $m = 1$, and vector components when $m = 0$. When we use the model at the resolution $N = 63$ and $J^0 = 64$ using the new DFS method in Sect. 5, we set $N = 63$ for each m except that we set $N = 62$ for $m = 0,1$, with Grid [−1]. We will describe this in the paper.

[4] Section 2.12 presents the Laplacian operator and the Poisson's equation. The accuracy of the new DFS method for these basic operators and others such as biharmonic diffusion operator should be addressed with detailed error magnitude. Also important is the global mean associated with the Poisson's equation.

The Laplacian operator and the Poisson equation is represented as

$$g = \nabla^2 f. \tag{R12}$$

Here, the global mean of g must be zero. Before calculating f from a given g in the Poisson equation, we should subtract the global mean from g (Cheong 2000b). We will describe this in the paper.

We examined the accuracy of the old and new DFS methods for the Laplacian operator in Eq. (R12) and the Helmholtz equation

$$h = (1-\varepsilon\nabla^2)f. \tag{R13}$$

Here, we give the function f as

$$f = \begin{cases} \frac{H}{4}\left(1+\cos\frac{\pi r}{R}\right)^2 & \text{if } r < R \\ 0 & \text{if } r \geq R \end{cases}, \tag{R14}$$

$$r = a\cos^{-1}[\sin\phi_c \sin\phi + \cos\phi_c \cos\phi \cos(\lambda-\lambda_c)], \tag{R15}$$

where $H = 1000$, $R = a/3$, ϕ is latitude, λ is longitude, a is the radius of the earth and r is the distance between (λ,ϕ) and the center $(\lambda_c,\phi_c) = (3\pi/2\,,\pi/2-0.05)$. The function f is similar to the cosine bell in the Williamson test case 1, but $(1+\cos\pi r/R)$ is squared so that the second derivative of f is continuous. To easily calculate the exact values of $\nabla^2 f$, the center is temporarily set to the North Pole, that is, $(\lambda_c,\phi_c) = (0,\pi/2)$ and $r = a\cos^{-1}[\sin\phi] = a\theta$, where θ is colatitude. At this time, g is calculated as follows:

$$g = \nabla^2 f = \frac{1}{a^2}\left[\frac{1}{\sin^2\theta}\frac{\partial^2 f}{\partial\lambda^2} + \frac{1}{\sin\theta}\frac{\partial}{\partial\theta}\left(\sin\theta\frac{\partial f}{\partial\theta}\right)\right]$$

$$= -\frac{\cos\theta}{\sin\theta}\frac{H}{2a^2}\frac{\pi a}{R}\left[\left(1+\cos\frac{\pi r}{R}\right)\sin\frac{\pi r}{R}\right] + \frac{H}{2a^2}\left(\frac{\pi a}{R}\right)^2\left[\sin^2\frac{\pi r}{R} - \left(1+\cos\frac{\pi r}{R}\right)\cos\frac{\pi r}{R}\right]. \tag{R16}$$

Equation (R16) is satisfied at any position of the center. The function h is calculated by

$$h = (1 - \varepsilon\nabla^2)f = f - \varepsilon g, \tag{R17}$$

where $\varepsilon = 0.01a^2$, and f and g are given by Eqs. (R14) and (R16).

To examine the accuracy for the Laplacian operator, f is given by (R14), and $\nabla^2 f$ is calculated from f with the old DFS method, the new DFS method (See Sect. 2.12) and the SH method. The calculated values are compared with the exact values of $\nabla^2 f$ in Eq. (16). Here, the exact values of $\nabla^2 f$ are truncated by the forward transform followed by the inverse transform in order to see the error that does not include the error due to the wavenumber truncation. Table R1 shows the root mean squared errors (RMSEs) between the calculated values and the exact values. The differences in error between the methods are small, and which is better depends on the resolution. Table R2 shows the global mean value of calculated $\nabla^2 f$. The exact value of the global mean of $\nabla^2 f$ is zero. In Table R2, the global mean values calculated with each method are very close to zero.

To examine the accuracy of the solution of the Helmholtz equation, h is given in Eq. (R17) and the Helmholtz equation in Eq. (R13) is solved with the old DFS method, the new DFS method (See Sect. 2.13) and the SH method. The calculated values are compared with the exact solution f in Eq. (R14). The exact values of f are also truncated as described above. Table R3 shows the RMSEs between the calculated values and the exact values. The difference in error between the methods are small, and which is better depends on the resolution and the arrangement of the grid points. This kind of accuracy test is important, and we will describe this in the paper or in the supplement.

	Old DFS [0]	New DFS [0],[1],[−1]	SH [Gaussian]
128x64, *N*=42	7.479772×10^{-13}	4.179854×10^{-13} 4.089208×10^{-13} 4.772618×10^{-13}	5.278089×10^{-13}
320x160, *N*=106	4.033842×10^{-14}	4.302001×10^{-14} 4.242989×10^{-14} 4.244875×10^{-14}	3.933373×10^{-14}
1920x960, *N*=639	4.407625×10^{-16}	6.478465×10^{-16} 6.514562×10^{-16} 6.478465×10^{-16}	4.257350×10^{-16}

Table R1. The RMSEs of Laplacian operator calculation ($\nabla^2 f$) with the old and new DFS methods and the SH method. In the new DFS method, the results of Grid [0], Grid [1] and Grid [−1] are shown in this order. The number of longitudinal (*I*) and latitudinal (*J*) grid points is shown in the form $I \times J$. *N* is the truncation wavenumber.

	Old DFS [0]	New DFS [0],[1],[-1]	SH [Gaussian]
128x64, *N*=42	2.766693×10^{-26}	1.474223×10^{-26} $-1.303193 \times 10^{-25}$ $-6.176935 \times 10^{-25}$	$-4.644813 \times 10^{-27}$
320x160, *N*=106	$-1.647899 \times 10^{-26}$	2.035640×10^{-26} 3.226382×10^{-25} $-4.130437 \times 10^{-25}$	3.004992×10^{-26}
1920x960, *N*=639	$-4.215168 \times 10^{-26}$	$-3.068185 \times 10^{-26}$ 2.356491×10^{-24} 4.677050×10^{-25}	9.469697×10^{-27}

Table R2. Same as Table R1 except that the global mean values of calculated $\nabla^2 f$ are shown.

	Old DFS [0]	New DFS [0],[1],[-1]	SH [Gaussian]
128x64, *N*=42	3.814822×10^{-2}	3.597815×10^{-2} 3.731604×10^{-2} 3.856617×10^{-2}	3.335080×10^{-2}
320x160, *N*=106	8.785639×10^{-4}	8.781645×10^{-4} 8.080622×10^{-4} 8.091810×10^{-4}	1.531216×10^{-3}
1920x960, *N*=639	2.193258×10^{-6}	2.193256×10^{-6} 1.937225×10^{-6} 1.945943×10^{-6}	1.918862×10^{-6}

Table R3. Same as Table R1 except that the RMSEs of the solution of the Helmholtz equation are shown.

[5] One of the most basic test case is the cosine-bell advection, which is not included in this manuscript. The test case is simple but useful to demonstrate the advantage and disadvantages of a numerical method.

The cosine-bell advection test case is certainly one of the most basic test cases. Since the advection equation is highly non-linear, it is challenging to solve the equation on the longitude-latitude grid using the Eulerian scheme with the DFS spectral method instead of the semi-Lagrangian scheme. We have run the Williamson test case 1 simulating the cosine-bell advection in the old DFS, new DFS, and SH Eulerian models. The advection equation is integrated by the leap-frog scheme with the Robert-Asselin time filter (Robert, 1969; Asselin, 1972) with a coefficient of 0.1. The horizontal diffusion is not used, but the zonal Fourier filter is used in the old and new DFS methods. In Eq. (76),

the value $M_0 = 20$ is used in the DFS shallow water models. However, the larger the value M_0 is, the higher the longitudinal resolution around the pole is. Because of this, when the Eulerian scheme is used and M_0 is large, a timestep must be very short due to the CFL condition. Therefore M_0 should be as small as possible. We have tested $M_0 = 0$, but this degrades the result of the Williamson test case 1. We have also tested $M_0 = 1$ and this result is good. Therefore, we use $M_0 = 1$ here.

Figure R1 shows the predicted height after a 12-day integration in the Williamson test case 1. The number of grid points is around 128 × 64. The truncation wavenumber *N* is 42 because the 2/3 rule (Orszag, 1971) is used in order to avoid aliasing in the nonlinear advection term. The timestep is 30 minutes. The results for DFS [0], DFS [1], DFS [-1] and SH are very similar. Instability occurs in the old DFS model without horizontal diffusion. Table R4 shows the errors of the predicted height after a 12-day integration in Williamson test case 1 (See Fig. 1) in the models at the resolution *N*=42 with around 128 × 64 grid points, and Table R5 shows the same as Table R4 except that the resolution is *N* = 639 with around 1920 × 960 grid points and the timestep is 150 seconds. The errors are very close among the models. At the resolution *N* = 639, the new DFS model without horizontal diffusion is unstable when the timestep is 200 seconds. The SH model without horizontal diffusion is stable when the timestep was 240 seconds and unstable when the timestep is 300 seconds. One reason for this difference in timestep is probably that the longitudinal resolution near the poles is higher in the new DFS model than in the SH model when $M_0 = 1$. When the fourth order horizontal diffusion in Eq. (100) is used, the both new DFS and SH models are stable when the timestep is 240 seconds and are unstable when the timestep is 300 seconds. The old DFS model is unstable even when the same fourth order horizontal diffusion is used. Higher-order horizontal diffusion, which effectively smooths out the high wavenumber components, stabilizes the Eulerian old DFS model (Cheong, 2000b; Cheong et al., 2002).

These results are very important and we will describe this in the paper.

Asselin, R. A.: Frequency filter for time integrations. Mon. Wea. Rev., 100, 487–490, 1972.

Robert, A. J.: The integration of a low order spectal form of the primitive meteorological equations. J. Meteor. Soc. Japan, 44, 237–245, 1966.

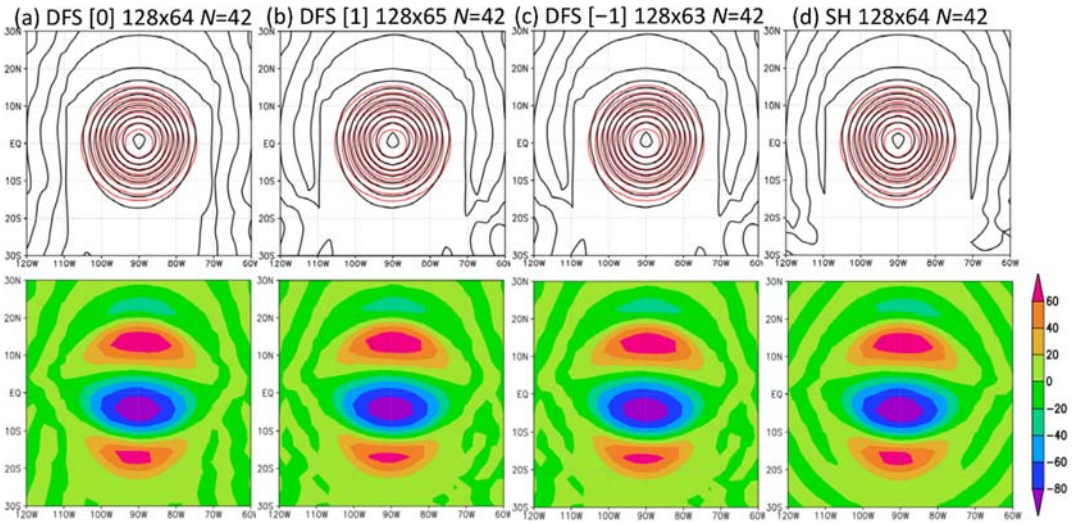

Figure R1. Predicted height (m) after a 12-day integration in Williamson test case 1. In the upper figures, the black contour shows the predicted height, and the red contour shows the reference solution. In the lower figures, color shading shows the difference between the predicted height and the reference solution.

	DFS Grid[0]	DFS Grid[1]	DFS Grid[-1]	SH Gaussian grid
L_1 error	0.16761	0.163979	0.164086	0.167435
L_2 error	0.115567	0.115594	0.115593	0.115539
L_{max} error	0.09711	0.0934617	0.0934646	0.0954416

Table R4. The error of predicted height after a 12-day integration in Williamson test case 1 (See Fig. 1). The number of grid points is around 128 × 64, and the truncation wavenumber N is 42.

	DFS Grid[0]	DFS Grid[1]	DFS Grid[-1]	SH Gaussian grid
L_1 error	0.00980851	0.00980841	0.00980842	0.00981044
L_2 error	0.00824238	0.00824238	0.00824238	0.00824238
L_{max} error	0.0067255	0.0067281	0.0067281	0.00672429

Table R5. Same as Table R4 except that the number of grid points is around 1920 × 960, and the truncation wavenumber *N* is 639.

[6] It is very nice to see that the simulations are carried out without numerical instability even without horizontal diffusion. The author may address why it is possible. Is it due to the diffusive property of the semi-Lagrangian?

One reason is due to the stability of the semi-Lagrangian scheme. Especially, the old DFS method

needs to use the semi-Lagrangian scheme for stability without horizontal diffusion. The new DFS method probably does not need to use the semi-Lagrangian scheme from the results obtained in the reply to the comment [5] above. We will add this explanation in the paper.

[7] Figure 2. The problem setting is quite strange. In principle, any scalar function with $m > 0$ should vanish at poles. Nevertheless, the 'original' function is given to have value of unity at north pole. Therefore, the computation and comparison are not meaningful.

In Figure 2, Grid [0] is used and there are no grid points at the poles. The original values are set to one at the grid points north of 30°N, and the value at the north pole is zero at the same time. This means that the original values abruptly change around the north pole. In the method of Cheong using Eq. (6), this abrupt change around the poles causes the large oscillations when the truncation wavenumber *N* for even $m\ (\geq 2)$ is lower than *J*. This explanation is necessary, and we will modify the explanation in Sect. 3.

[8] Figure 5. Result of DFS0 appears to be too much smooth compared to DFS_old. Why is it?

This is because the least squares method is used to calculate the expansion coefficients in DFS [0]. In Fig. 2, the number of latitudinal grid points J is 64, and the truncation wavenumber N is 63. Figure R2(a) shows the same figure as Fig. 2(a) except that $J = 64$ and $N = 63$. When $N = 63$, in the old DFS method using the Cheong's basis functions in Eq. (6), we set $N = 63$ for $m = 0$, and $N = 64$ for $m \neq 0$. Because $N = J$ for even $m\ (\geq 2)$, the forward transform followed by the inverse transform does not change the original values at the grid points, and the oscillations do not appear in the old DFS method. Fig. R2(b) is the same as Fig. R2(a) except that it also shows the values between grid points calculated from the expansion coefficients by using Eq. (6) or Eq. (8). The large oscillations appear in the old DFS method, and it makes the latitudinal derivative at the grid points large. This is probably one reason that high zonal wavenumber noise appears near the noise in the old DFS model without horizontal diffusion. In the new DFS method, only small ocillations appear in Fig. R2(b) because the error is minimized by using the least squares method when calculating the expansion coefficients. We think that this is important and we will add this explanation and Fig. R2 in this paper.

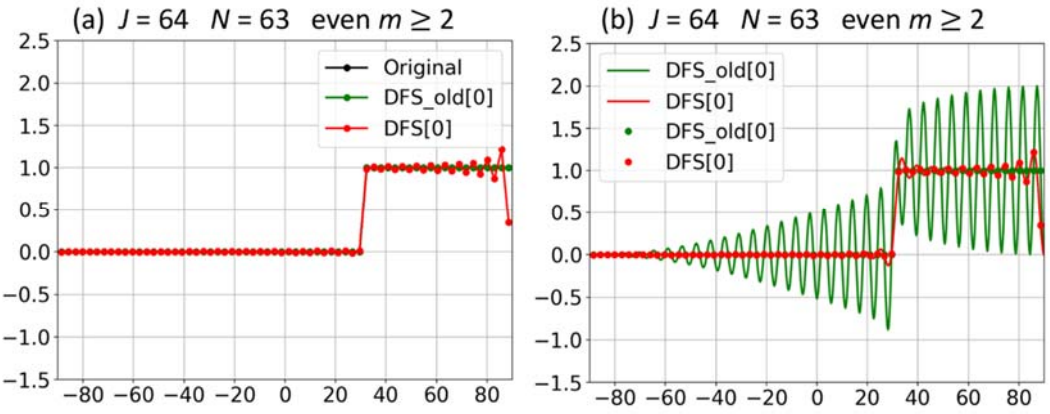

Figure. R2. Change in values due to the meridional wavenumber truncation for even $|m|$ (≥ 2). We use Grid [0] with the number of latitudinal grid points $J = 64$. Original values (black) are meridionally transformed from grid space to spectral space, truncated with $N = 63$, and transformed back from spectral space to grid space. Green: Cheong's expansion method. Red: the new expansion method. (a) Values at the grid points. (b) Values at the grid points and between grid points calculated from the expansion coefficients.

Specific minor comments

[1] The right hand side of (25) should be represented with matrix-vector multiplication as in the left hand side.

Thank you for the advice. We will modify Eq. (25).

[2] Terms associated with $\tilde{T}^{c,J}_{1,m}$ and $\tilde{T}^{c,J}_{1,m}$ in (36) do not appear in (37). The reason should be explained.

I am sorry this is a typo. The right equation for Eq. (37) is

$$E^{\mathrm{SH}} = \frac{1}{2}\int_0^{\pi}\left[\left(T^{\mathrm{c,SH},N}_{m=0}(\theta) - \tilde{T}^{c,J}_{m=0}(\theta)\right)^2 + \frac{1}{2}\sum_{m=1}^{M}\left(T^{\mathrm{c,SH},N}_{m}(\theta) - \tilde{T}^{c,J}_{m}(\theta)\right)^2 + \frac{1}{2}\sum_{m=1}^{M}\left(T^{\mathrm{s,SH},N}_{m}(\theta) - \tilde{T}^{s,J}_{m}(\theta)\right)^2\right]\sin\theta\, d\theta. \quad \text{(R18)}$$

[3] Equation (B1) can be found in Cheong 2000a.

We have forgotten to cite Cheong 2000a. We will fix it.